Microchimica Acta (2021) 188: 350
https://doi.org/10.1007/s00604-021-05015-5

ORIGINAL PAPER

Ultrasensitive dual-quenching electrochemiluminescence immunosensor for prostate specific antigen detection based on graphitic carbon nitride quantum dots as an emitter

Pingkun Liu[1] · Hui Meng[1] · Gui Zhang[1] · Li Song[1] · Qian Han[1] · Cun Wang[1] · Yingzi Fu[1]

Received: 5 June 2021 / Accepted: 1 September 2021 / Published online: 23 September 2021

Abstract

Early monitoring of prostate-specific antigen (PSA) is crucial in diagnosis and proactive treatment of prostate disease. Herein, a dual-quenching ternary ECL immunosensor was designed for PSA detection based on graphitic carbon nitride quantum dots (g-CNQDs, as an emitter), potassium persulfate ($K_2S_2O_8$, as a coreactant), and silver nanoparticles doped multilayer Ti_3C_2 MXene hybrids (Ag@TCM, as a coreaction accelerator). First, Ag@TCM was immobilized on the surface of a glassy carbon electrode, then g-CNQDs was further adsorbed on Ag@TCM to acquire a higher initial ECL signal at a potential window from − 1.3 to 0.0 V (vs. Ag/AgCl). Ag@TCM not only acted as the coreaction accelerator, but also as a matrix to load enormous g-CNQDs and prostate-specific capture antibody via Ag–N bond. Meanwhile, prostate-specific detection antibody was marked by gold nanoparticles modified manganese dioxide as a dual-quenching probe (Ab2- Au@MnO_2). When Ab2-Au@MnO_2 was introduced into the ternary ECL system via sandwiched immuno-reaction, the high-sensitive detection of PSA was achieved by the dual-quenching effect, caused by the resonant energy transfer from g-CNQDs (energy donor) to Au@MnO_2 (energy acceptor). As a result, this ECL immunosensor showed a good dynamic concentration range from 10 fg·mL^{-1} to 100 ng·mL^{-1} with a detection limit of 6.9 fg·mL^{-1} for PSA detection. The dual-quenching ECL strategy presented high stability and good specificity to open up a new pathway for ultrasensitive immunoassay.

Keywords Electrochemiluminescence · Dual-quenching effect · Gold nanoparticles modified manganese dioxide · Graphitic carbon nitride quantum dots · Silver nanoparticles doped multilayer Ti_3C_2 MXene hybrids · Immunosensor

Introduction

Prostate-specific antigen (PSA) is a biomarker for clinical diagnosis of prostate cancer. The normal threshold for PSA in serum is less than 4 ng·mL^{-1}, while the abnormal level of cancer patients is up to 10 ng·mL^{-1} [1]. It is significant for developing sensitive, accurate, and specific PSA detection techniques for early diagnosis and the improvement of survival rate of cancer patients. Many methods have been implemented for PSA detection, such as electrochemistry [2], chemiluminescence [3], fluorescence [4], photoelectrochemistry [5], and electrochemiluminescence (ECL) [6]. ECL sensing technology with the merits of high sensitivity and controllability, low background, easy operation, and wide dynamic range has attracted the attention of researchers [7, 8].

Quenching type sensors, as one of the most important ECL model, mainly rely on high initial ECL intensity and good quenching material to obtain satisfactory detection results. On the one hand, different signal amplification strategies can be employed, including the use of chemical or enzymatic catalysis, the introduction of nanoparticles or active micro-molecules as coreaction accelerators [9], even the utilization of some materials with large specific surface areas as carriers to load enormous emitters [10, 11]. On the other hand, various quenchers have been involved in the fabrication of ECL biosensors, of which the resonant energy transfer (RET) from ECL emitter (energy donor) to quencher (energy acceptor) is an important means to achieve the quenching effect [12, 13]. Exploring suitable ECL emitter

✉ Yingzi Fu
fyzc@swu.edu.cn

[1] Key Laboratory of Luminescence Analysis and Molecular Sensing (Southwest University), Ministry of Education, School of Chemistry and Chemical Engineering, Southwest University, Chongqing 400715, China

as acceptor or quencher as donor to construct an ECL sensor is an extremely interesting and challenging work.

Graphite-carbon nitride (g-C_3N_4), as a layered metal-free semiconductor, has attracted tremendous attention in the virtue of low cytotoxicity, stable chemical properties, excellent photoelectric properties, and low cost [14, 15]. Typically, the synthesis of bulk g-C_3N_4 is achieved by pyro-condensation of nitrogen-rich organic precursors. However, as a result of the potential accumulation of polymer layers during the production process, the surface area and solubility of polymer layers are restricted, resulting in poor conductivity and low quantum yield [16]. These problems can be well addressed in two approaches: reducing dimensions and combining with carbon materials [17–20]. For example, small size graphite-carbon nitride quantum dots (g-CNQDs) not only retain the structure of bulk g-C_3N_4, but also possess large specific surface area, high optical stability, quantum confinement effect, and good water solubility [21, 22]. Meanwhile, dramatic results can be gotten by combining g-C_3N_4 with other carbon materials (such as graphene, carbon nanotubes). As an emerging layered two-dimensional (2D) carbon material, MXenes show superior performance in terms of specific surface area, conductivity, catalytic ability, and biocompatibility [23–26]. Ti_3C_2 MXene (TCM) is a matrix used to immobilize biomolecules in fluorescent and electrochemical sensors, and also as a coreaction accelerator for signal enhancement [27, 28]. Manganese dioxide (MnO_2) nanomaterials have a broad absorption (200–600 nm) and a large specific surface area, which can effectively play the role of a luminescence quencher owing to the wide-range overlapping between the absorption of MnO_2 and the emission of emitters [29].

Herein, a sandwich ternary ECL system was constructed based on g-CNQDs as an ECL emitter, $K_2S_2O_8$ as a coreactant, and silver nanoparticles doped TCM (Ag@TCM) as coreaction accelerator. Ag@TCM acted as a matrix to load a large number of g-CNQDs and prostate-specific capture antibodies (Ab1). Meanwhile, prostate-specific detection antibody (Ab2) was marked by gold nanoparticles (Au) modified MnO_2 to be a dual-quenching probe (Ab2-Au@MnO_2). A highly sensitive and specific PSA ECL immunosensor triggered by the dual-quenching effect deriving from the resonant energy transfer (RET) between donor (g-CNQDs) and accepter (Au@MnO_2, accepter1: Au and accepter2: MnO_2), which realized a dual-quenching for g-CNQDs.

Experimental section

Reagents and materials

Melamine, polyvinylpyrrolidone (PVP), poly-(diallyldimethylammoniumchloride) (PDDA), silver nitrate ($AgNO_3$), manganese dioxide (MnO_2), ethylene glycol (EG, 99%), sodium citrate, potassium persulfate ($K_2S_2O_8$), and chloroauric acid ($HAuCl_4{\cdot}4H_2O$) were supplied by the Chemical Reagent Co. (Chongqing, China). Ti_3C_2 MXene (TCM) was gained from Nanjing Xianfeng nanomaterials Co., Ltd. Prostate-specific antigen (PSA), prostate-specific antibody (Ab), carcinoembryonic antigen (CEA), alpha fetoprotein (AFP), and bovine serum albumin (BSA) were obtained from J&K Chemical Co. (Beijing, China). Human serum was obtained from the Ninth People's Hospital of Chongqing, China. 0.1 M phosphate-buffered saline (PBS) containing K_2HPO_4, NaH_2PO_4, and KCl was used throughout the whole work. All reagents and chemicals were of analytical grade and aqueous solutions were prepared with deionized water (18.2 MΩ·cm).

Apparatus

The ECL measurements were carried out on an MPI-E electrochemiluminescence analyzer (Remex Electronic Science and Technology Co. Ltd., Xi'an, China). Electrochemical impedance spectroscopy (EIS) measurements were carried out at the CHI 604 D electrochemical workstation (Shanghai Chenhua Instruments Co, China). Scanning electron microscopy (SEM, Hitachi Instruments Co., Japan) and transmission electron microscopy (TEM, JEM-1200EX, Japan) were used to record the morphologies and size of various materials. The X-ray photoelectron spectra (XPS) of the materials were measured by a VG Scientific ESCALAB 250 spectrometer (Thermoelectricity Instruments, USA). UV–vis absorption spectra were recorded by using UV-2600 spectrophotometer (Shimadzu, Japan). The three-electrode system was used for detection: a bared or modified glassy carbon electrode (GCE, $\Phi = 4$ mm) as a working electrode, a platinum wire as a counter electrode, and an Ag/AgCl (sat. KCl) electrode as a reference electrode.

Synthesis of g-CNQDs

The graphitic carbon nitride quantum dots (g-CNQDs) were prepared via micromechanical exfoliation [21]. The process is mainly divided into four steps (Scheme 1A): first, 3 g of melamine was heated in the muffle furnace at 550 °C for 4 h to form bulk g-C_3N_4. Second, 1 g of bulk g-C_3N_4 was treated by using concentrated sulfuric acid (20 mL) and nitric acid (20 mL) for about 2 h at room temperature. The resulting white product was washed with water three times and isolated by centrifuge to get porous g-C_3N_4 (Figure S1). Third, 100 mg of the porous g-C_3N_4 was dispersed in 30 mL ammonia, then the mixture was transferred into a 45-mL teflon-sealed autoclave and heated at 120 °C for 12 h, during which the porous g-C_3N_4 was peeled into sheets. After cooling to room temperature, the residue was washed with water for

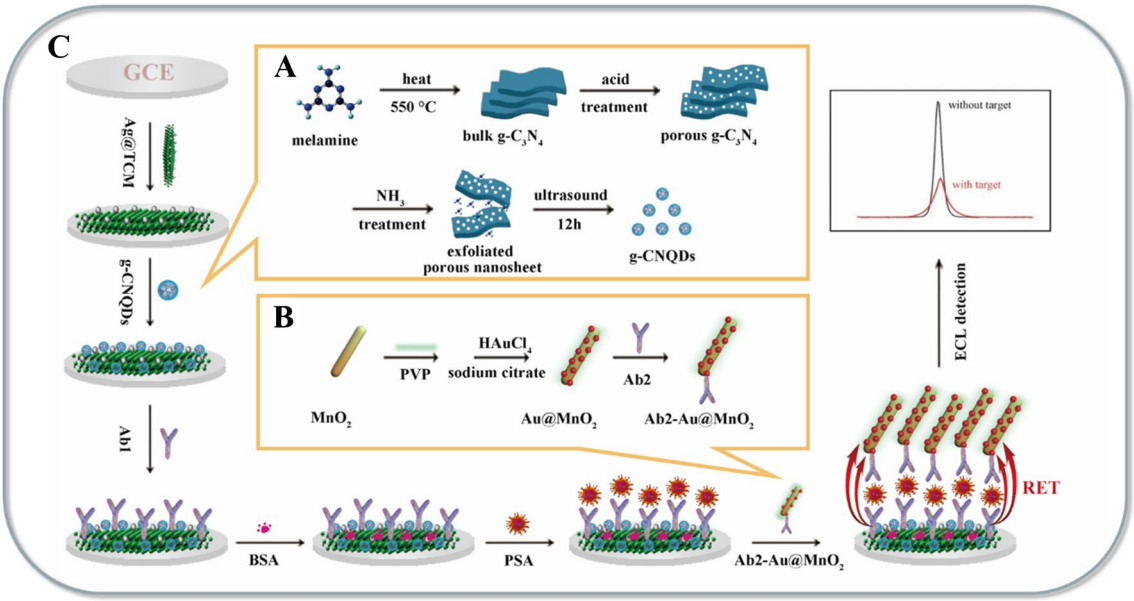

Scheme 1 Preparation of **A** g-CNQDs and **B** Ab2-Au@MnO_2 quenching probe. **C** Construction process of the dual-quenching ECL immunosensor

several times and dried in room temperature. Fourth, 100 mg of residue was dispersed in 100 mL water and sonicated for 6 h. Then, the suspension was separated by centrifuge at 7000 rpm. The g-CNQDs were obtained by dialysis of the aqueous suspension to remove large-sized particles.

Synthesis of Ag@TCM

A layer-by-layer assembly approach has been used to prepare silver nanoparticles doped multilayer Ti_3C_2 MXene hybrids (Ag@TCM). First, 1 mL of PDDA (1%, a cationic polyelectrolyte) was mixed with 1 mL of TCM suspension (0.5 mg/mL) to obtain positively charged TCM [30]. Subsequently, 0.5 mL of silver nanoparticles dispersion (1 mg/mL, synthesized according to literature [31], negatively charged) was added into the above TCM suspension and kept stirring for 3 h. The unnecessary PDDA was removed through washing and centrifugation. Through the oppositely charged interaction, Ag@TCM were collected and redispersed in water to acquire Ag@TCM dispersion (0.5 mg/mL) for further use.

Preparation of dual-quenching probe

Five milligrams of MnO_2 powder was dispersed in 5 mL water, then 1 mL of $HAuCl_4$ (1%) and 3 mg of PVP were mixed with MnO_2 and stirred for 6 h. After that, 2 mL of 50 mM sodium citrate solution was added dropwise to reduce $HAuCl_4$. After stirring for 24 h, the gold nanoparticles modified MnO_2 was obtained by washing and centrifuge thrice, and redispersed into 5 mL water (Au@MnO_2, Scheme 1B). Afterwards, 0.4 mL of prostate-specific detection antibody (Ab2, 10 μg/mL) was added into 1 mL of Au@MnO_2 (1 mg/mL) suspension under stirring for 24 h at 4 °C. Followed by centrifuging, the Au@MnO_2 marked Ab2 (Ab2-Au@MnO_2, quenching probe) was obtained, dispersed in 1 mL of 0.1 M PBS (pH 7.4), and stored at 4 °C.

Fabrication of the ECL immunosensor

The ECL immunosensor was constructed as follows (Scheme 1C). Ten microliters of Ag@TCM and 6 μL of as-prepared g-CNQDs were dropped onto the cleaned surface of GCE successively and dried at room temperature (GCE/Ag@TCM/g-CNQDs). Subsequently, 3 μL of prostate-specific capture antibody (Ab1, 10 μg/mL) was dropped on the modified electrode surface and incubated at 4 °C for 2 h (GCE/Ag@TCM/g-CNQDs/Ab1). Following that, 5 μL of BSA (1 wt%) was incubated for 1 h to block nonspecific binding sites (GCE/Ag@TCM/g-CNQDs/Ab1/BSA). Then, 6 μL of PSA with different concentrations was added and further incubated at 4 °C for 2 h (GCE/Ag@TCM/g-CNQDs/Ab1/BSA/PSA). At last, 6 μL of Ab2-Au@MnO_2 was added and incubated for 2 h (GCE/Ag@TCM/g-CNQDs/Ab1/BSA/PSA/Ab2-Au@MnO_2). The electrode was rinsed with 0.1 M PBS (pH 7.4) after each step of modification. The other control electrodes were prepared in a similar way.

The ECL measurement was performed in 0.1 M PBS (3 mL) containing 5 mM $K_2S_2O_8$. The voltage of the photomultiplier tube was set at 600 V and the measurement

potential was set from – 1.3 to 0.0 V (vs. Ag/AgCl) with a scan rate of 200 mV/s.

Results and discussion

Characterization of different materials

The TEM image indicates that a uniform diameter of g-CNQDs dispersed on the matrix is 2.5 nm (Fig. 1A). The high-resolution (HR)-TEM image reveals the crystal lattice spacing of the quantum dots is about 0.23 nm (upper inset of Fig. 1A). The SEM image of TCM presents an accordion-like layered structure (Fig. 1B). Figure 1C shows some small particles scattered on the TCM surface. And g-CNQDs are adsorbed on the Ag@TCM surface (Fig. 1D). Figure 1F depicts the energy-dispersive X-ray analysis (EDX) mapping images, showing that the elements of Ti, C, N, and Ag are the primary components of the Ag@TCM/g-CNQDs. In addition, the SEM image of Au@MnO_2 exhibits that gold nanoparticles are uniformly distributed on MnO_2 surface via in situ reduction growth method (Fig. 1E).

Moreover, the chemical compositions and elemental valence states of the g-CNQDs was investigated by XPS spectrum. The full survey spectrum of g-CNQDs indicates the coexistence of C, N, and O elements (Fig. 2A). The four peaks of C 1 s at 284.83, 286.02, 288.03, and 288.49 eV in HR-XPS are corresponding to the bond structures of C–C, C–O–C, N–C = N, and O–C = O, respectively, manifesting their surficial functional groups (Fig. 2B). The N 1 s displays three components, including 398.56, 399.55, and 401.1 eV in response to C–N = C, N–$(C)_3$, and –NH_3/ = NH (Fig. 2C). Similarly, O 1 s region can be fitted to three peaks in the regions of 529.54, 530.55, and 531.82 eV, which can be assigned to O–H, C–O, and C = O, respectively (Fig. 2D). There is a good agreement between these findings and earlier reports of g-CNQDs [21].

Possible ECL mechanisms of the different systems

The three-dimensional (3D) surface image of ECL-potential-wavelength (Fig. 3A) and 3D heat map image (Fig. 3S) of g-CNQDs were recorded in 5 mM $K_2S_2O_8$ solution (0.1 M PBS, pH 7.4). They all indicate that a stable ECL blue-light emission of g-CNQDs at 460 nm. The ECL behaviors of GCE/g-CNQDs and GCE/Ag@TCM were investigated by cyclic potential scanning from – 1.3 to 0.0 V in 0.1 M PBS (pH 7.4) with or without 5 mM $K_2S_2O_8$. As can be seen in Fig. 3B, weak ECL signals are observed on GCE/g-CNQDs (curve a) and GCE/Ag@TCM (curve b) in PBS. Meanwhile, when $K_2S_2O_8$ is present, except a small ECL signal is appeared on bare GCE (curve c), the successively enhanced ECL intensities are obtained on the GCE/Ag@TCM (curve d), GCE/g-CNQDs (curve e), and GCE/Ag@TCM/g-CNQDs (curve f). A very high ECL signal is gotten on GCE/g-CNQDs (curve e), indicating that g-CNQDs owns the potential to be used as a good ECL emitter. Especially when g-CNQDs (emitter), $K_2S_2O_8$ (coreactant), and

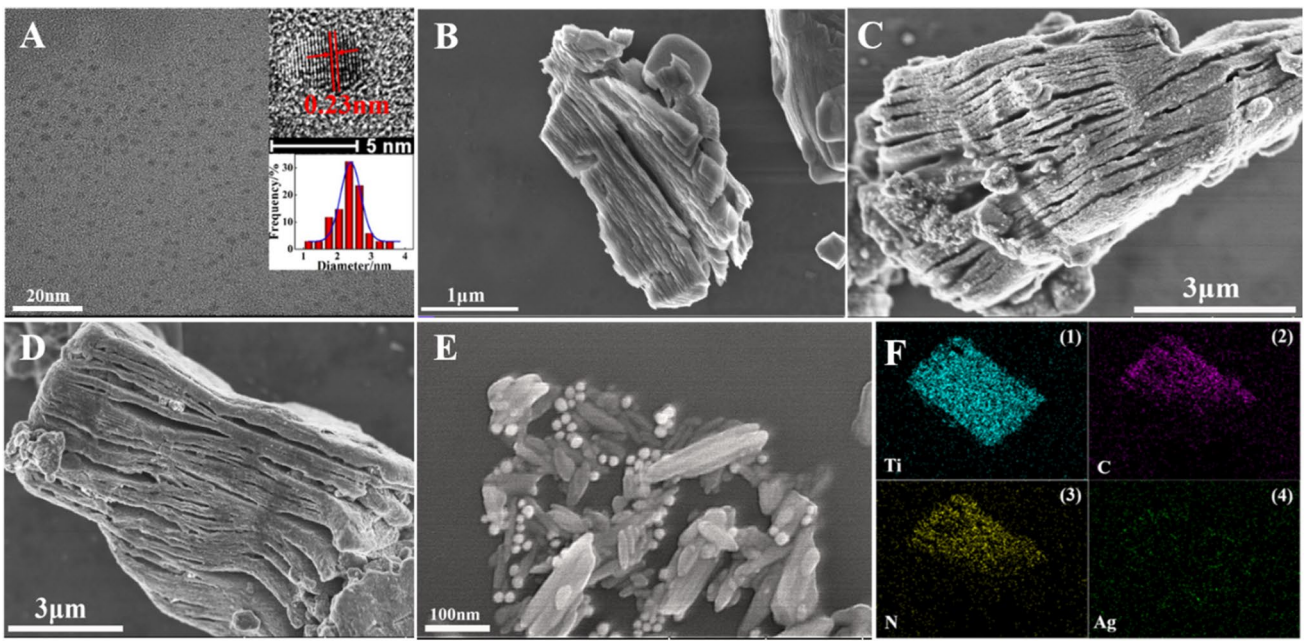

Fig. 1 **A** TEM image of g-CNQDs (upper inset: lattice fringe image; lower inset: diameter distribution). SEM images of **B** TCM, **C** Ag@TCM, **D** Ag@TCM/g-CNQDs, and **E** Au@MnO_2. **F** EDX mapping of Ag@TCM/g-CNQDs

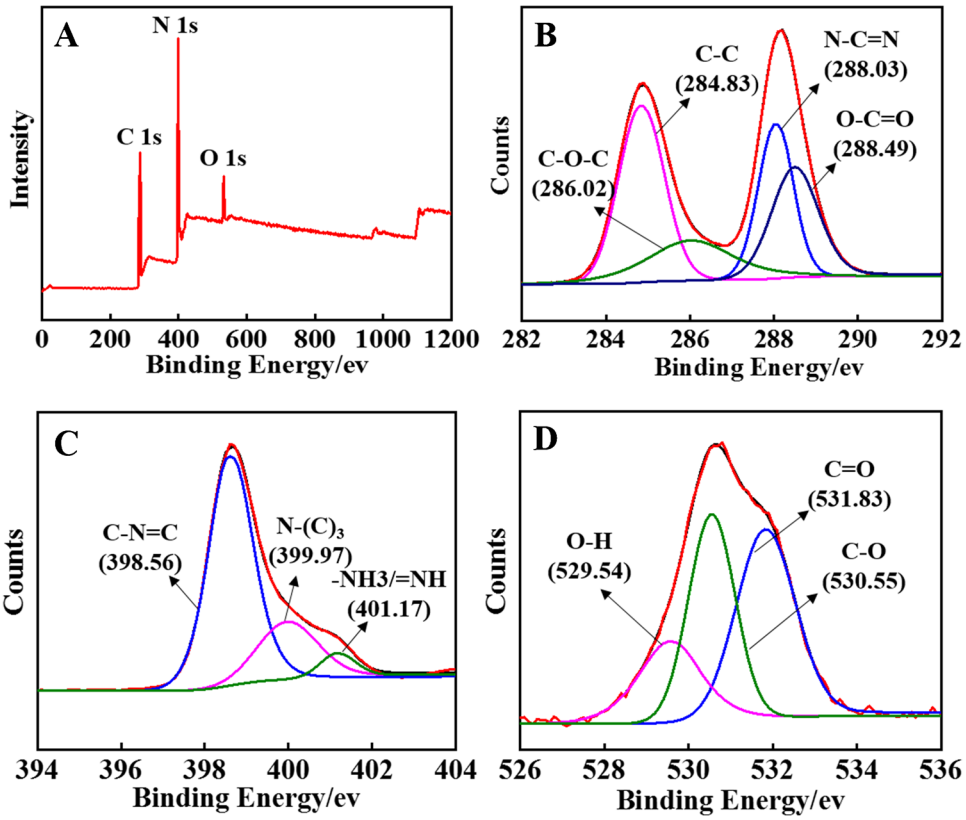

Fig. 2 **A** The XPS full spectrum of g-CNQDs. The HR-XPS spectra of **B** C 1 s, **C** N 1 s, and **D** O 1 s

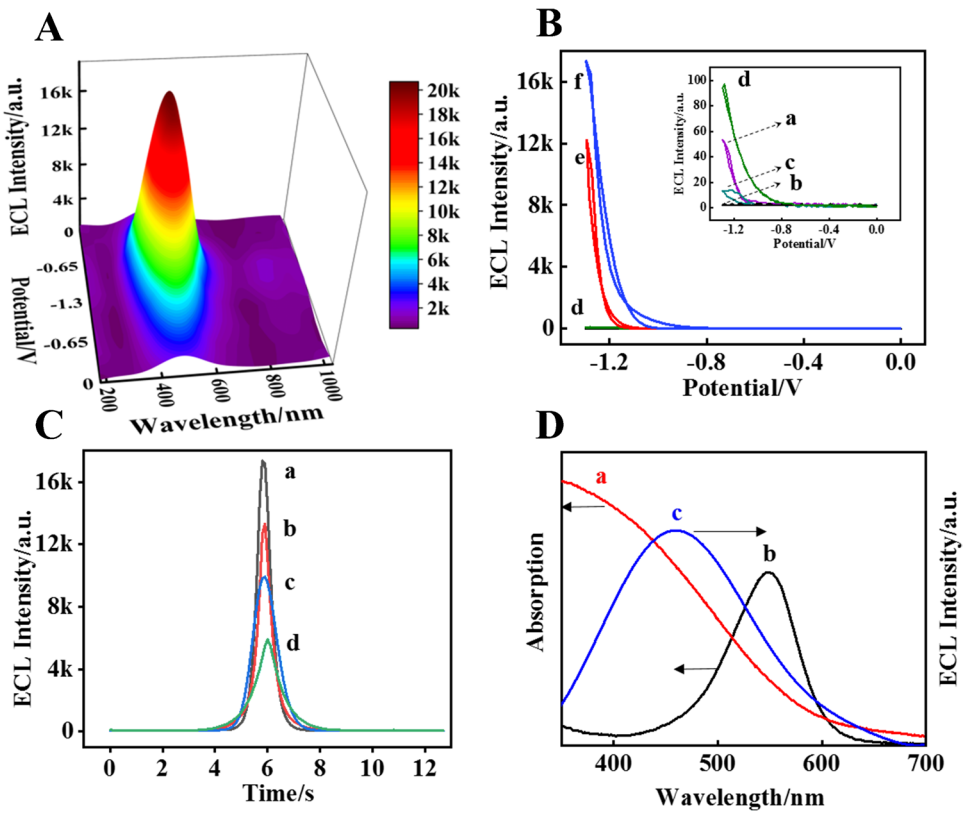

Fig. 3 **A** 3D surface image of ECL-potential-wavelength of g-CNQDs. **B** ECL intensity vs. potential curves of (a) GCE/g-CNQDs and (b) GCE/Ag@TCM in 0.1 M PBS (pH 7.4); (c) bare GCE, (d) GCE/Ag@TCM, (e) GCE/g-CNQDs, (f) GCE/Ag@TCM/g-CNQDs in 5 mM $K_2S_2O_8$ solution (0.1 M PBS, pH 7.4). **C** ECL intensity-time curves of (a) GCE/Ag@TCM/g-CNQDs, (b) GCE/Ag@TCM/g-CNQDs/Au, (c) GCE/Ag@TCM/g-CNQDs/MnO_2, and (d) GCE/Ag@TCM/g-CNQDs/Au@MnO_2. **D** UV–vis absorption spectra of (a) MnO_2 and (b) Au, ECL emission spectrum of (c) g-CNQDs

Ag@TCM (coreaction accelerator) coexist to form a ternary system, the ECL intensity on GCE/Ag@TCM/g-CNQDs is significantly improved (curve f).

The possible ECL mechanism of Ag@TCM/g-CNQDs/$K_2S_2O_8$ system was discussed [32]. When the GCE/g-CNQDs was swept from − 1.3 to 0.0 V, g-CNQDs and $S_2O_8^{2-}$ were reduced to g-CNQDs$^{\cdot-}$ and $SO_4^{\cdot-}$, respectively. Subsequently, the $SO_4^{\cdot-}$ reacted with the g-CNQDs$^{\cdot-}$ to generate the excited state g-CNQDs*. Finally, g-CNQDs* returned to the ground state and an intense emission was obtained (see Eq. 1–4):

$$g-CNQDs + e^- \rightarrow g-CNQDs^{\bullet-} \quad (1)$$

$$S_2O_8^{2-} + e- \rightarrow SO_4^{2-} + SO_4^{\bullet-} \quad (2)$$

$$SO_4^{\bullet-} + g-CNQDs^{\bullet-} \rightarrow g-CNQDs^* + SO_4^{2-} \quad (3)$$

$$g-CNQDs^* \rightarrow g-CNQDs + h\nu \quad (4)$$

In addition, the role of Ag@TCM/g-CNQDs, gold nanomaterials (Au), and MnO_2 in the proposed ECL system was investigated. As shown in Fig. 3C, GCE/Ag@TCM/g-CNQDs shows a high ECL response (curve a), suggesting that Ag@TCM/g-CNQDs as an emitter has good ECL performance. When further modified by Au (GCE/Ag@TCM/g-CNQDs/Au, curve b) or MnO_2 (GCE/Ag@TCM/g-CNQDs/MnO_2, curve c), the ECL intensity decrease significantly, hinting a certain quenching effect. The largest decrease of ECL intensity occurred after the modification of Au@MnO_2 (GCE/Ag@TCM/g-CNQDs/Au@MnO_2, curve d), implying Au@MnO_2 can be used as a good quencher. The UV–vis absorption spectra of the quencher and ECL spectrum of the emitter were further used to research the quenching effect between Au@MnO_2 and g-CNQDs. As evidenced in Fig. 3D, the UV–vis absorption spectra of MnO_2 (curve a) and Au (curve b) are overlapped appropriately with the ECL emission spectrum of g-CNQDs (curve c), indicating the RET existed in g-CNQDs (donor) and Au (acceptor), g-CNQDs (donor) and MnO_2 (acceptor). That is to say, the dual-quenching effect of Au@MnO_2 on g-CNQDs ECL system is confirmed.

Characterization of the developed ECL immunosensor

The ECL behavior of different modified electrodes was studied in 5 mM $K_2S_2O_8$ (0.1 M PBS, pH 7.4). As depicted in Fig. 4A, almost no ECL signal is obtained on bare GCE (curve a), while a very strong ECL response is observed on GCE/Ag@TCM/g-CNQDs with the help of $K_2S_2O_8$

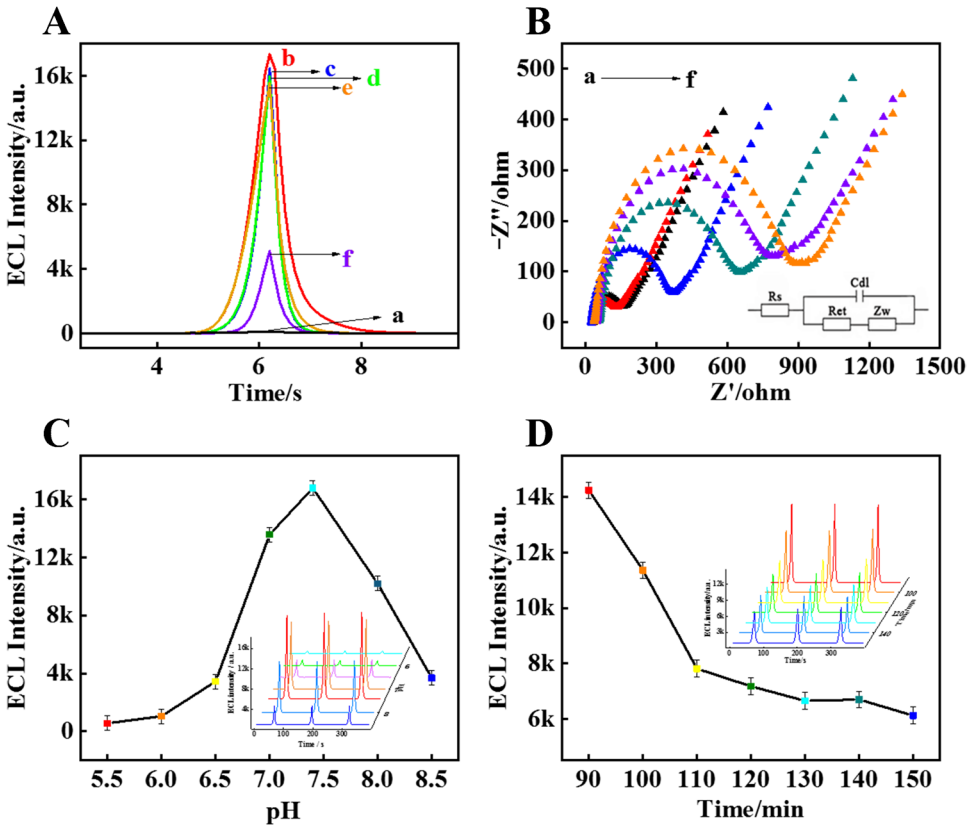

Fig. 4 **A** ECL behavior in 5 mM $K_2S_2O_8$ (0.1 M PBS, pH 7.4) and **B** EIS of (a) bare GCE, (b) GCE/Ag@TCM/g-CNQDs, (c) GCE/Ag@TCM/g-CNQDs/Ab1, (d) GCE/Ag@TCM/g-CNQDs/Ab1/BSA, (e) GCE/Ag@TCM/g-CNQDs/Ab1/BSA/PSA, and (f) GCE/Ag@TCM/g-CNQDs/Ab1/BSA/PSA/Ab2-Au@MnO_2. Effects of **C** pH and **D** incubation time for Ab2-Au@MnO_2, error bars: standard deviation (SD), $n = 3$

(coreactant) and Ag@TCM (coreaction accelerator) (curve b). Due to the electron-blocking properties of proteins, the ECL intensities decreased in turn when Ab1, BSA, and PSA were successively added on the modified electrode (curves c to e). When the quenching probe Ab2-Au@MnO_2 was introduced via immune response, the signal is severely quenched (curve f). This is attributed to the RET effect between g-CNQDs (donor) and Au@MnO_2 (acceptor).

EIS was also used to characterize the fabrication of different modified electrodes (Fig. 4B). Compared with the bare GCE (curve a), no significant change of electron transfer resistance (R_{et}) is observed on GCE/Ag@TCM (curve b), indicating that Ag@TCM has good conductivity. With the modification of Ab1, BSA, PAS, and Ab2-Au@MnO_2 successively, the R_{et} increase in sequence (curves c to f). Since the proteins contained in Ab1, BSA, PSA, and Ab2 obstruct electron transfer seriously.

Optimization of the detection conditions

An appropriate experimental condition is vital to the performance of immunosensors. The influence of pH from 5.5 to 9.5 was investigated (Fig. 4C). ECL intensity reaches the maximum in a neutral environment (pH 7.4), so 7.4 was chosen as the optimum pH. Moreover, the incubation time of Ab2-Au@MnO_2 onto the surface of the immunosensor was studied from 90 to 110 min (Fig. 4D). The ECL intensity decline sharply with the increase of incubation time. After the incubation time more than 110 min, the changes of intensity slow down. So, 110 min was selected in subsequent experiments.

Performances of the ECL immunosensor

When Ab2-Au@MnO_2 was incubated on the surface of immunosensor, a sandwich immune response was triggered. Figure 5 shows the ECL intensity decrease as the increasing PSA concentration from 10 fg·mL^{-1} to 100 ng·mL^{-1}. A good linear dynamic response between ECL intensity and the logarithmic concentration of PSA. The linear relation is $I = 5332.8 - 2337.6 \times \lg c$ ($R^2 = 0.994$) with a limit of detection (LOD) of 6.9 fg·mL^{-1} (S/N = 3) [33].

As listed in Table 1, this immunosensor exhibited a better analytical performance. Compared with previous reports, this dual-quenching ternary ECL immunosensor performed a broader detection range and a much lower LOD, which may provide strong support for early diagnosis of prostate cancer. Moreover, the use of g-CNQDs as ECL emitter instead of expensive luminous materials insures that it is easily available and low cost. Though the sandwich-type ternary ECL immunosensor is somehow complicated compared with references [34] and [35], this strategy provides a detection specificity and significantly improves the sensitivity based on the introduction of Ag@TCM. It is important

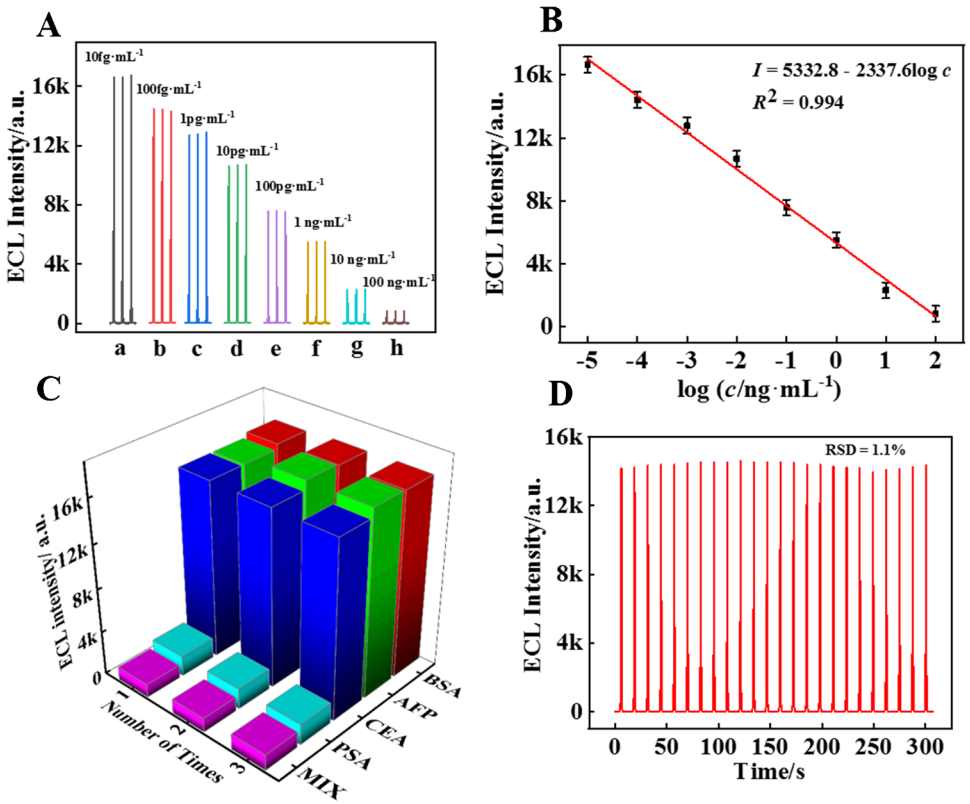

Fig. 5 **A** ECL response for different PSA concentration in 5 mM $S_2O_8^{2-}$ (0.1 M PBS). **B** The calibration curve for the ECL intensity vs. the logarithm of PSA concentration, error bars: SD, $n = 3$. **C** Selectivity and **D** stability of the ECL immunosensor

Table 1 Comparison assay of various strategies for PSA detection

Detection system	Methods	Linear range	Detection limit	Ref
hollow@SiO_2@SiO_2-RuBpy	FL	100 pg·mL^{-1}–100 ng·mL^{-1}	27 pg·mL^{-1}	[36]
Apt/Luminol/$HPSiO_2$	CL	1 pg·mL^{-1}–100 ng·mL^{-1}	270 fg·mL^{-1}	[34]
AuE/MCH/PCOOH/Zr(IV)/BPAA/Fc	SWV	341 fg·mL^{-1}–341 pg·mL^{-1}	109 pg·mL^{-1}	[2]
NH_2-CuO/BSA/P-Pep-RhB/β-CD/$AgInS_2$	PEC	0.1 pg·mL^{-1}–100 ng·mL^{-1}	60 fg·mL^{-1}	[37]
Au NPs/(Fc@MgAl-LDH)n-Ab1	ECL	50 fg·mL^{-1}–50 ng·mL^{-1}	34 fg·mL^{-1}	[3]
Ag^+@UIO-66-NH_2/CdWS/Ab1	ECL	0.1 pg·mL^{-1}–10 ng·mL^{-1}	38 fg·mL^{-1}	[38]
MNP/Ab1-PSA-Ab2/L@MIL-53(Fe)	ECL	5 pg·mL^{-1}–200 ng·mL^{-1}	100 fg·mL^{-1}	[35]
Ag@TCM/g-CNQDs/Ab1	ECL	10 fg·mL^{-1}–100 ng·mL^{-1}	6.9 fg·mL^{-1}	This work

to highlight that this strategy for PSA detection is skillfully to use Ag@TCM as coreaction accelerator and Au@MnO_2 as dual-quenching probe in ECL technique.

FL, fluorescence; *CL*, chemiluminescence; *SWV*, square wave voltammograms; *PEC*, photoelectrochemistry; *ECL*, electrochemiluminescence; *RuBpy*, Tris(2,2-bipyridyl) dichlororuthenium(II) hexahydrate; *Apt/Luminol/HPSiO$_2$*, hollow porous silica encapsulated luminol by aptamers; *P-Pep-RhB*, the part of peptide and rhodamine B; *AgInS$_2$*, silver indium sulfide; *Fc@MgAl-LDH*, ferrocenecarboxylic acid@MgAl layered double hydroxides; *MNPs*, magnetic nanoparticles; *L@MIL-53(Fe)*, luminol loaded within the MIL-53(Fe)-NH_2.

Selectivity and stability were explored to assess the analytical performance. Bovine albumin (BSA), alpha fetoprotein (AFP), and carcinoembryonic antigen (CEA) with the same concentration of 1 μg·mL^{-1} were selected as possible interfering species to assess the selectivity of the immunosensor. As evidenced by Fig. 5C, no obvious change is appeared on the ECL responses when detecting the mixed sample (1 μg·mL^{-1} aforementioned interferences and 0.1 μg·mL^{-1} PSA) and 0.1 μg·mL^{-1} PSA. These results demonstrate the noticeable selectivity of this ECL immunosensor for PSA detection. The stability of the immunosensor was evaluated by determining 0.1 pg·mL^{-1} PSA during continuous scans for 25 cycles. As shown in Fig. 5D, there is no significant undulation (relative standard deviation, RSD = 1.1%), indicating the excellent stability of this immunosensor. In addition, after 15 days of the storage (4 °C), 8.7% decrease in ECL intensity is observed for 0.1 pg·mL^{-1} PSA. Meanwhile, five modified electrodes in the same batch were utilized to detect 0.1 pg·mL^{-1} PSA; the RSD was 4.1%.

Table 2 Recovery tests for PSA in the diluted human serum samples (n = 6)

Sample	Added	Found	RSD (%)	Recovery (%)
1	10 ng·mL^{-1}	10.5 ng·mL^{-1}	2.2	105.1
2	100 pg·mL^{-1}	102 pg·mL^{-1}	1.5	102.0
3	1 pg·mL^{-1}	0.96 pg·mL^{-1}	2.6	96.0

These results showing the immunosensor possessed acceptable stability and reproducibility.

Application in real samples

To evaluate the feasibility of this ECL immunosensor for real sample detection, the healthy human serum samples were selected. Prior to using, the samples were centrifuged to get the supernatant. Then each sample was diluted 100-fold with 0.1 M PBS (pH = 7.4) and spiked PSA with different concentrations (1 pg·mL^{-1}, 100 pg·mL^{-1}, and 10 ng mL^{-1}). Under the same conditions as the standard sample, the ECL analyses were executed in 3 mL sample solution including 5 mM $S_2O_8^{2-}$ (0.1 M PBS). The results are listed in Table 2, and the recovery rates are in the range of 96.0–105.1% with RSD from 1.5 to 2.6% (n = 6), indicating that this strategy can be effectively used for PSA detection in real sample.

Conclusion

In conclusion, a dual-quenching ECL immunosensor has been skillfully prepared for ultrasensitive detection of PSA. This ternary ECL system consisted of g-CNQDs, $K_2S_2O_8$, and Ag@TCM as the emitter, coreactant, and coreaction accelerator, respectively. With the help of Ag@TCM and $K_2S_2O_8$, a high ECL intensity was obtained. Owning to the double quenching effect from Au and MnO_2 in Au@MnO_2, ECL intensity achieved a satisfied quenching detection of PSA. This ECL immunosensor exhibited acceptable sensitivity, selectivity, and stability in the determination of PSA, demonstrating a promising quenching strategy in ECL sensing and a wide application prospects in early cancer diagnosis. However, non-reusability is a limitation of this sensor, which is going to be a challenge for us in the later stages.

Supplementary Information The online version contains supplementary material available at https://doi.org/10.1007/s00604-021-05015-5.

Funding This work was supported by the National Natural Science Foundation of China (22077105) and the Natural Science Foundation Project of CQ CSTC (cstc2020jcyj-msxmX0854).

Declarations

Conflict of interest The authors declare no competing interests.

References

1. Liang H, Xu HB, Zhao YT, Zheng J, Zhao H, Li GL, Li CP (2019) Ultrasensitive electrochemical sensor for prostate specific antigen detection with a phosphorene platform and magnetic covalent organic framework signal amplifier. Biosens Bioelectron 144:111691
2. Hu Q, Gan SY, Bao Y (2020) Zhang YW,* Han DX, Niu L (2020) Electrochemically controlled ATRP for cleavage-based electrochemical detection of the prostate-specific antigen at femtomolar level concentrations. Anal Chem 92:15982–15988
3. Liu A, Zhao F, Zhao Y, Guan LS, Liu S (2016) A portable chemiluminescence imaging immunoassay for simultaneous detection of different isoforms of prostate specific antigen in serum. Biosens Bioelectron 81:97–102
4. Rong Z, Bai Z, Li J, Tang H, Shen T, Wang Q, Wang CW, Xiao R, Wang SQ (2019) Dual-color magnetic-quantum dot nanobeads as versatile fluorescent probes in test strip for simultaneous point-of-care detection of free and complexed prostate-specific antigen. Biosens Bioelectron 145:111719
5. Zeng R, Zhang L, Su L, Luo Z, Zhou Q, Tang D (2019) Photoelectrochemical bioanalysis of antibiotics on rGO-Bi_2WO_6-Au based on branched hybridization chain reaction. Biosens Bioelectron 133:100–106
6. Zhang YC, Zhang Z, Wang ZM, Pan HZ, Lin Y, Chang D (2021) Sensitive detection of prostate-specific antigen based on dual signal amplification of Fc@MgAl-LDH and NH_2-MIL-101(Fe). Biosens Bioelectron 190:113437
7. Wang HJ, Liao LL, Chai YQ, Yuan R (2020) Sensitive immunosensor based on high effective resonance energy transfer of lucigenin to the cathodic electrochemiluminescence of tris(bipyridine) Ru(II) complex. Biosens Bioelectron 150:111915
8. Fang DD, Zhang SP, Dai H, Lin YY (2019) An ultrasensitive ratiometric electrochemiluminescence immunosensor combining photothermal amplification for ovarian cancer marker detection. Biosens Bioelectron 146:111768
9. Zhou Y, Chen SH, Luo XL, Chai YQ, Yuan R (2018) Ternary electrochemiluminescence nanostructure of Au nanoclusters as a highly efficient signal label for ultrasensitive detection of cancer biomarkers. Anal Chem 90:10024–10030
10. Khan MS, Ameer H, Ali A, Li Y, Yang L, Ren X, Wei Q (2020) Electrochemiluminescence behaviour of silver/$ZnIn_2S_4$/reduced graphene oxide composites quenched by Au@SiO_2 nanoparticles for ultrasensitive insulin detection. Biosens Bioelectron 162:112235
11. Zhao G, Wang Y, Li X, Yue Q, Dong X, Du B, Cao W, Wei Q (2019) Dual quenching electrochemiluminescence strategy based on 3D metal-organic frameworks for ultrasensitive detection of amyloid-β. Anal Chem 91:1989–1996
12. Song C, Li XJ, Hu LH, Shi TF, Wu D, Ma HM, Zhang Y, Fan DW, Wei Q, Ju HX (2020) Quench-type electrochemiluminescence immunosensor based on resonance energy transfer from carbon nanotubes and Au-nanoparticles-enhanced g-C_3N_4 to CuO@Polydopamine for procalcitonin detection. ACS Appl Mater Interfaces 12:8006–8015
13. Liu Y, Haghighatbin MA, Shen W, Cui H (2020) Functionalized polydopamine nanospheres with chemiluminescence and immunoactivity for label-free copeptin immunosensing. ACS Applied Nano Materials 3:4681–4689
14. Hu LY, Zheng J, Zhao K, Deng AP, Li JG (2018) An ultrasensitive electrochemiluminescent immunosensor based on graphene oxide coupled graphite-like carbon nitride and multiwalled carbon nanotubes-gold for the detection of diclofenac. Biosens Bioelectron 101:260–267
15. Liu JL, Jiang J, Zhang JQ, Chai YQ, Xiao Q, Yuan R (2020) The combination of ternary electrochemiluminescence system of g-C_3N_4 nanosheet/TEA/Cu@Cu_2O and G-quadruplex-driven regeneration strategy for ultrasensitive bioanalysis. Biosens Bioelectron 152:112006
16. An T, Tang J, Zhang YY, Quan Y, Gong X, Al-Enizi AM, Elzatahry AA, Zhang LJ, Zheng GF (2016) Photoelectrochemical conversion from graphitic C_3N_4 quantum dot decorated semiconductor nanowires. ACS Appl Mater Interfaces 8:12772–12779
17. Sudhaik A, Raizada P, Thakur S, Saini AK, Hosseini-Bandegharaei A (2020) Metal-free photo-activation of peroxymonosulfate using graphene supported graphitic carbon nitride for enhancing photocatalytic activity. Mater Lett 277:128277
18. Boldaji SR, Yaftian MR, Hatefi-Mehrjardi A, Shayani-Jam H (2020) Graphitic carbon nitride-graphene nanoplates; application in the sensitive electrochemical detection of noscapine. Synth Met 268:116489
19. Liu ZM, Zhang X, Ge XG, Hu LQ, Hu YJ (2019) Electrochemiluminescence sensing platform for ultrasensitive DNA analysis based on resonance energy transfer between graphitic carbon nitride quantum dots and gold nanoparticles. Sens. Actuators B Chem 297:126790
20. Zhou M, Weng Q, Popov ZI, Yang Y, Antipina LY, Sorokin PB, Wang X, Bando Y, Golberg D (2018) Construction of polarized carbon–nickel catalytic surfaces for potent, durable, and economic hydrogen evolution reactions. ACS Nano 12:4148–4155
21. Zhang X, Wang H, Wang H, Zhang Q, Xie J, Tian Y, Wang J, Xie Y (2014) Single-layered graphitic-C(3)N(4) quantum dots for two-photon fluorescence imaging of cellular nucleus. Adv Mater 26:4438–4443
22. Fageria P, Uppala S, Nazir R, Gangopadhyay S, Chang CH, Basu M, Pande S (2016) Synthesis of monometallic (Au and Pd) and bimetallic (AuPd) nanoparticles using carbon nitride (C_3N_4) quantum dots via the photochemical route for nitrophenol reduction. Langmuir 32:10054–10064
23. Naguib M, Mochalin VN, Barsoum MW, Gogotsi Y (2013) MXenes: a new family of two-dimensional materials. Adv Mater 26:992–1005
24. Chen JL, Tong P, Huang LT, Yu ZH, Tang DP (2019) Ti_3C_2 MXene nanosheet-based capacitance immunoassay with tyramine-enzyme repeats to detect prostate-specific antigen on interdigitated micro-comb electrode. Electrochim Acta 319:375–381
25. Fang YF, Yang XC, Chen T, Xu GF, Liu ML, Liu JQ, Xu YH (2018) Two-dimensional titanium carbide (MXene)-based solid-state electrochemiluminescent sensor for label-free single-nucleotide mismatch discrimination in human urine. Sens Actuators B Chem 263:400–407
26. Lorencova L, Bertok T, Filip J, Jerigova M, Velic D, Kasak P, Mahmoud KA, Tkac J (2018) Highly stable Ti_3C_2Tx (MXene)/Pt nanoparticles-modified glassy carbon electrode for H_2O_2 and small molecules sensing applications. Sens Actuators B Chem 263:360–368
27. Zhang H, Wang Z, Zhang Q, Wang F, Liu Y (2019) Ti_3C_2 MXenes nanosheets catalyzed highly efficient electrogenerated chemiluminescence biosensor for the detection of exosomes. Biosens Bioelectron 124–125:184–190

28. Mohammadniaei M, Koyappayil A, Sun Y, Min J, Lee MH (2020) Gold nanoparticle/MXene for multiple and sensitive detection of oncomiRs based on synergetic signal amplification. Biosens Bioelectron 159:112208
29. Su Q, Gan LL, Zhu Y, Yang XM (2021) Dual-emissive fluorescence and phosphorescence detection of cholesterol and glucose based on carbon dots-cyanuric acid complex quenched by MnO_2 nanosheets. Sens Actuators B Chem 335:129715
30. Ma MN, Zhuo Y, Yuan R, Chai YQ (2015) New signal amplification strategy using semicarbazide as co-reaction accelerator for highly sensitive electrochemiluminescent aptasensor construction. Anal Chem 87:11389–11397
31. Zuo F, Zhang C, Zhang H, Tan X, Chen S, Yuan R (2019) A solid-state electrochemiluminescence biosensor for Con A detection based on CeO_2@Ag nanoparticles modified graphene quantum dots as signal probe. Electrochim Acta 294:76–83
32. Wang H, Ma Q, Wang YF, Wang CH, Qin DD, Shan DL, Chen J, Lu XQ (2017) Resonance energy transfer based electrochemiluminescence and fluorescence sensing of riboflavin using graphitic carbon nitride quantum dots. Anal Chim Acta 973:34–42
33. Chen AY, Zhao M, Zhuo Y, Chai YQ, Yuan R (2017) Hollow porous polymeric nanospheres of a self-enhanced ruthenium complex with improved electrochemiluminescent efficiency for ultrasensitive aptasensor construction. Anal Chem 89:9232–9238
34. Sun YL, Gao P, Han R, Luo CN, Wei Q (2021) A target-triggered signal chemiluminescence sensor for prostate specific antigen detection based on hollow porous silica encapsulated luminol by aptamers. Sens Actuators B Chem 333:129543
35. Khoshfetrat SM, Khoshsafar H, Afkhami A, Mehrgardi MA, Bagheri H (2019) Enhanced visual wireless electrochemiluminescence immunosensing of prostate-specific antigen based on the luminol loaded into MIL-53(Fe)-NH_2 accelerator and hydrogen evolution reaction mediation. Anal Chem 91:6383–6390
36. Xu DD, Deng YL, Li CY, Lin Y, Tang HW (2017) Metal-enhanced fluorescent dye-doped silica nanoparticles and magnetic separation: a sensitive platform for one-step fluorescence detection of prostate specific antigen. Biosens Bioelectron 87:881–887
37. Fu YM, Xiao K, Zhang XH, Du CC, Chen JH (2021) Peptide cleavage-mediated and environmentally friendly photocurrent polarity switching system for prostate-specific antigen assay. Anal Chem 93:1076–1083
38. Fang Q, Lin Z, Lu F, Chen Y, Gao W (2019) A sensitive electrochemiluminescence immunosensor for the detection of PSA based on CdWS nanocrystals and Ag^+@UIO-66-NH_2 as a novel coreaction accelerator. Electrochim Acta 302:207–215